Geophysical Journal (1988) **95**, 1–13

Source parameters of seven large Australian earthquakes determined by body waveform inversion

Joanne Fredrich and Robert McCaffrey*
Department of Earth, Atmospheric and Planetary Sciences, Massachusetts Institute of Technology, Cambridge, MA 02139, USA

David Denham
Australian Seismological Centre, Bureau of Mineral Resources, GPO Box 378, Canberra ACT 2601, Australia

Accepted 1988 March 7. Received 1988 February 1; in original form 1987 June 11

SUMMARY

We determine source mechanisms and centroid depths for the seven largest earthquakes in and near the Australian continent in the past 20 yr using teleseismic body waves. Six of the earthquakes were thrusts and one was strike-slip. All five earthquakes that occurred beneath the continent were shallower than 10 km (the ranges of centroid depths are constrained to be 1–5, 2–4, 0–3, 5–11, and 6–10 km) and indicate nearly pure thrust faulting. The three shallowest events were associated with surface faulting. While the published first motion solutions for these three events included large amounts of strike-slip, our thrust mechanisms are more consistent with displacements observed at the surface of the Earth. The range of possible centroid depths for a strike-slip earthquake beneath the continental shelf off the northwest coast is 23–29 km, and that for a thrust earthquake in oceanic lithosphere beneath the Tasman Sea is 22–26 km below sea level. The pressure axis is consistently near-horizontal, and in the western half of the continent, five earthquakes indicate that the azimuth of the maximum compressive stress is E–ENE (azimuthal range of 66°–91°). On the basis of one earthquake, we conclude that the *P*-axis is oriented NNW beneath the Tasman Sea.

Key words: Australia, earthquake source mechanism, intraplate seismicity

1 INTRODUCTION

Although the Earth's seismic activity is concentrated at plate boundaries, stable intraplate regions occasionally produce large earthquakes. The seismic radiation of an earthquake contains information about principal stress directions and, thus, the study of such intraplate events can help us to understand certain geodynamic processes, including the driving forces for plate tectonics (e.g. Sykes & Sbar 1973; Fitch, Worthington & Everingham 1973; Richardson, Solomon & Sleep 1979). Understanding earthquakes also contributes to the better assessment of seismic hazards in a region.

The continent of Australia, generally considered to be tectonically stable, has been the site of large earthquakes in recent and historic times. Nine earthquakes of body wave magnitude greater than 5.6 have occurred in the continent in the 20 years prior to 1987, the largest being the Meckering earthquake in 1968 with a surface wave magnitude of 6.8. As in many regions, detailed understanding of Australian seismicity has been hampered by the short record of seismicity—prior to about 1960 the network of seismic stations was too sparse to permit the reliable location of small seismic events (Doyle & Underwood 1965). Determination of the depth of faulting has also been problematic, especially for those events in northwestern and central Australia where no local seismic networks exist. Depth estimates for shallow focus earthquakes can be in error by tens of kilometers in the absence of nearby stations (e.g. Jackson 1980).

Lambeck *et al.* (1984) summarize fault plane solutions in the literature for Australian earthquakes of local magnitude ≥ 2.5. Although the solutions consistently yield roughly horizontal compression axes, there is considerable variation in the azimuth of *P*-axes over very short distances. *In situ* stress measurements (Denham, Alexander & Worotnicki 1979) using overcoring techniques corroborate the existence of a horizontal maximum compressive stress. However, the measurements have been made only at very shallow depths (<10 m); therefore it is uncertain whether or not they are indicative of stresses at depth. Thus, it has been difficult to define regional stress orientations in the Australian continent on the basis of the first motion solutions and *in situ* stress measurements.

In this study, we constrain the fault plane solutions, depths, seismic moments, and source time functions of the seven largest earthquakes in Australia in the past 20 years using teleseismic body waveforms (these do not include three events near Tennant Creek on 1988 January 22 that

* Now also at: Air Force Geophysical Laboratory, Hanscom AFB.

occurred after this study was completed). Fault plane solutions based on *P*-wave first motions have been published for five of the events, two have been studied using their teleseismic body waves, and four have had centroid-moment tensor solutions determined. In comparison to *P*-wave first motions, body waveforms yield a more robust focal mechanism solution, and also provide reliable information on the centroid depth, the scalar seismic moment, and the source time function. The centroid-moment tensor method of Dziewonski & Woodhouse (1983) yields reliable mechanisms for large earthquakes, but the low frequency data used are not sensitive to depth for shallow events (i.e. <20 km). Depths for the events with first motion solutions are based on phase arrival-times and are associated with uncertainties of tens of kilometers (McCaffrey 1988). By studying the body waves of the large Australian earthquakes, our aim is to obtain a set of well-constrained fault plane solutions, depths, and seismic moments that will increase understanding of the contemporary seismicity.

2 AUSTRALIAN SEISMICITY

The western part of the Australian continent, which was cratonized in the Archean, experiences high levels of seismicity (Fig. 1). The two largest earthquakes studied here (1968 October 14 and 1979 June 2), both of which had $M_s \geq 6.0$, occurred in the southwest corner of the continent. Seismicity is distributed diffusely throughout western Australia and extends offshore into a geologically complex area of Phanerozoic basins and plateaus (Veevers 1984). One of the events studied here (1979 April 23) occurred beneath one of these offshore basins. There is no clear association of seismicity with known geologic structures, and faults that bound the major geological provinces do not appear to be active. In particular, a N-trending 1000 km long fault in the southwest corner of the continent (Fig. 1) is apparently aseismic.

In south-central Australia, earthquakes are mostly small (i.e. $M_L < 3$) and less than 5 km in depth (Stewart and Mount 1972). Seismicity is generally associated with the Adelaide geosyncline, which formed from the late Precambrian to early Palaeozoic. Farther north, four earthquakes of local magnitude >5 have occurred in the Simpson Desert area (24°S, 136°E) over the past 50 years, including one of the earthquakes studied here (1972 August 28).

Most seismic activity in eastern Australia is less than 20 km depth (Doyle 1968) and confined to orogenic belts of Paleozoic and Mesozoic ages. Although some small earthquakes have been associated with known faults (e.g. Bock & Denham 1983), the seismicity does not correlate with known tectonic structures. Off the southeast coast, a concentration of seismicity in the oceanic lithosphere of the Tasman Sea near 40°S, 157°E includes the event of 1983 November 11 studied here.

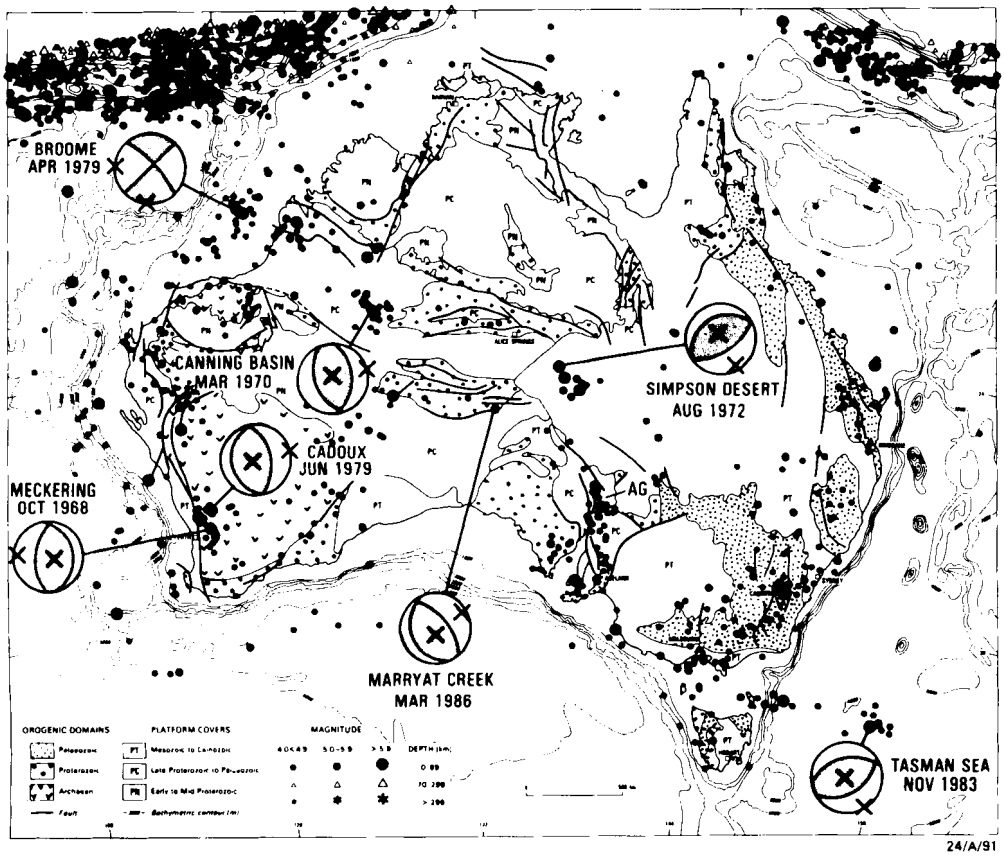

Figure 1. Epicenters of earthquakes with magnitude 4 or greater in the Australian region for the period 1973–1985. Fault plane solutions for the earthquakes studied here are also shown. Compressional quadrants are filled and the pressure (*P*) and tension (*T*) axes are indicated with crosses, with the *T*-axis bisecting the compressional quadrant.

Table 1. Epicentral data[a] and source parameters[b] for earthquakes studied.

No.	Date	Origin time (hr:min:sec)	Lat. (°S)	Long. (°E)	M	M_0 (10^{18} Nm)	Strike (°)	Dip (°)	Rake (°)	Depth (km)	D^c	P-axis (Az, pl)
1	1968 Oct. 14	2:58:51.8	31.54	117.00	6.8[d]	10.40 ± 0.53	351 ± 10	29 ± 7	73 ± 10	1–5	5.4	273, 17
2	1979 June 2	9:47:58.7	30.73	117.21	6.0[d]	1.49 ± 0.34	171 ± 10	34 ± 7	98 ± 10	2–4	6.4	75, 11
3	1986 March 30	8:53:53.2	26.19	132.77	5.8[d]	0.58 ± 0.15	148 ± 20	35 ± 20	80 ± 25	0–3	4.0	66, 10
4	1970 March 24	10:35:16.8	22.08	126.65	5.9[d]	1.17 ± 0.13	161 ± 5	45 ± 10	80 ± 5	5–11	3.0	78, 1
5	1972 Aug. 28	2:18:59.4	25.01	136.37	5.6[e]	0.10 ± 0.02	55 ± 40	60 ± 10	90 ± 40	6–10	1.8	145, 15
6	1979 April 23	5:45:09.8	16.66	120.16	5.7[d]	1.46 ± 0.49	225 ± 5	88 ± 5	171 ± 5	23–29	3.2	271, 5
7	1983 Nov. 25	19:57:18.0	40.45	155.61	5.9[d]	1.29 ± 0.24	54 ± 5	48 ± 10	75 ± 5	22–24	3.4	155, 2

[a] Source: International Seismological Centre Bulletin.
[b] Errors in centroid depth and the stike, dip, and rake angles are estimated uncertainties (see text) and errors in moment are formal errors of two standard deviations.
[c] Duration in seconds (time in which 95 per cent of the seismic moment is released).
[d] Surface wave magnitude.
[e] Body wave magnitude.

3 EARTHQUAKE SOURCE MECHANISMS

We determine best-fitting double-couple point sources and the associated uncertainties for seven earthquakes (Table 1 and Fig. 1) using a body waveform inversion technique based on the method for modelling far-field displacements due to a point-dislocation (Langston & Helmberger 1975; Nabelek 1984, 1985; McCaffrey & Nabelek 1984). In order to avoid complexities in the waveforms caused by upper mantle and core-mantle boundary structures, only seismograms from stations in the epicentral distance ranges of 30°–90° for P-waves and 30°–70° for SH-waves are used. The synthetic seismograms are generated by combining direct (P or S) and reflected (pP and sP, or sS) phases. The inversion adjusts the model to minimize residuals between the observed and synthetic seismogram amplitudes in the least squares sense. The adjusted parameters are the orientation (strike and dip) of one of the nodal planes and the rake on that plane, the centroid depth, and the relative amplitudes of elements of the source time function, which is parameterized by a series of overlapping isosceles triangles (Nabelek 1984). Anelastic attenuation is described by a t^* (the ratio of travel time to average Q) of 1 s and 4 s for long period P- and SH-waves, respectively (Futterman 1962), and 0.7 s for short period P-waves. In our approach, the orientation and centroid depth are not sensitive to the value of t^* chosen because we realign synthetic and observed seismograms by cross-correlation and because the systematic effects of varying t^* are absorbed by the source duration and to a lesser degree by the seismic moment (Nabelek 1984; Nelson, McCaffrey & Molnar 1987). Receiver structures are assumed to be a homogeneous half space and the source structures for each event are given in Table 2.

Table 2. Crustal structure used in calculation of seismograms.

Event no.	V_p (km s^{-1})	V_s (km s^{-1})	Density (g cm^{-3})	Depth to top of layer (km)
1, 2, 3, 4	6.0	3.4	2.8	0
5	3.2	1.8	2.4	0
	6.0	3.4	2.8	4.5
6	1.5	0	1.0	0
	4.5	2.5	2.5	0.5
	6.5	3.7	2.5	8.5
7	1.5	0	1.0	0
	6.4	3.7	2.9	4.5
	8.0	4.6	3.3	11.5

The majority of data used in the inversion are hand digitized, long period analogue records from the World Wide Standardized Seismograph Network (WWSSN), interpolated at intervals of 0.25 s, and long period seismograms from the Global Digital Seismograph Network (GDSN). Short period analogue and digital records interpolated at 0.1 and 0.5 s, respectively, are also included in the inversion for two events (nos. 3 & 5). In general, the misfit between the observed and synthetic waveforms is due to errors in the source and receiver crustal structure, unmodelled path effects, rupture propagation, and station background noise. Only noise that is coherent will effect the solution so that receiver structure and background noise are unimportant sources of error. Effects of unmodelled structure near the source and along the ray path are decreased by inverting the P and SH seismograms from all stations simultaneously. With long-period data, a point source (i.e. all slip occurs at the same point in space but not in time) is a valid approximation for earthquakes of the size of those considered here (Nabelek 1984; McCaffrey 1988). Nevertheless, we attempted to model the larger or more complicated events with multiple subevents of different orientations and depths but in none of the cases did a significant improvement to the fit of the seismograms result. Vogfjord & Langston (1987) also showed that the long period seismograms for the largest earthquake studied here (the Meckering event) are not sensitive to the direction of propagation. Complex events with the same double-couple orientation are allowed by the parameterization of the source time function.

3.1. Event 1: 1968 October 14, Meckering

This event occurred in the SW corner of the continent (Fig. 1) and, with the possible exception of the largest of the January 1988 events (McCaffrey & Fredrich, unpubl.), was the largest earthquake in Australia in the past quarter century. It produced surface breakage over roughly 200 km^2 and a N-trending fault scarp nearly 37 km long with a maximum observed dip-slip of 3.5 m and an average slip of 2 m in the east-side-up sense (Gordon & Lewis 1980). Numerous aftershocks occurred in the following months and

an event of $M_L = 5.9$ occurred about 80 km to the NW roughly 18 months later, again accompanied by significant surface faulting. Body waves from this second event proved to be too small to be studied with our technique.

The best-fitting mechanism indicates almost pure thrust faulting on a N-striking plane (Fig. 2a) and the centroid depth is 3 km. The east-side-up displacement in the surface faulting suggests that the shallower, E-dipping nodal plane is the fault plane. Visual comparison of the synthetic to observed waveforms indicates agreement for ranges in strike, dip, and rake angles of ±10°, ±7°, and ±10°, respectively. Using a moment tensor inversion technique, Vogfjord & Langston (1987) obtained a best-fitting double-couple solution that is similar to ours (differences in

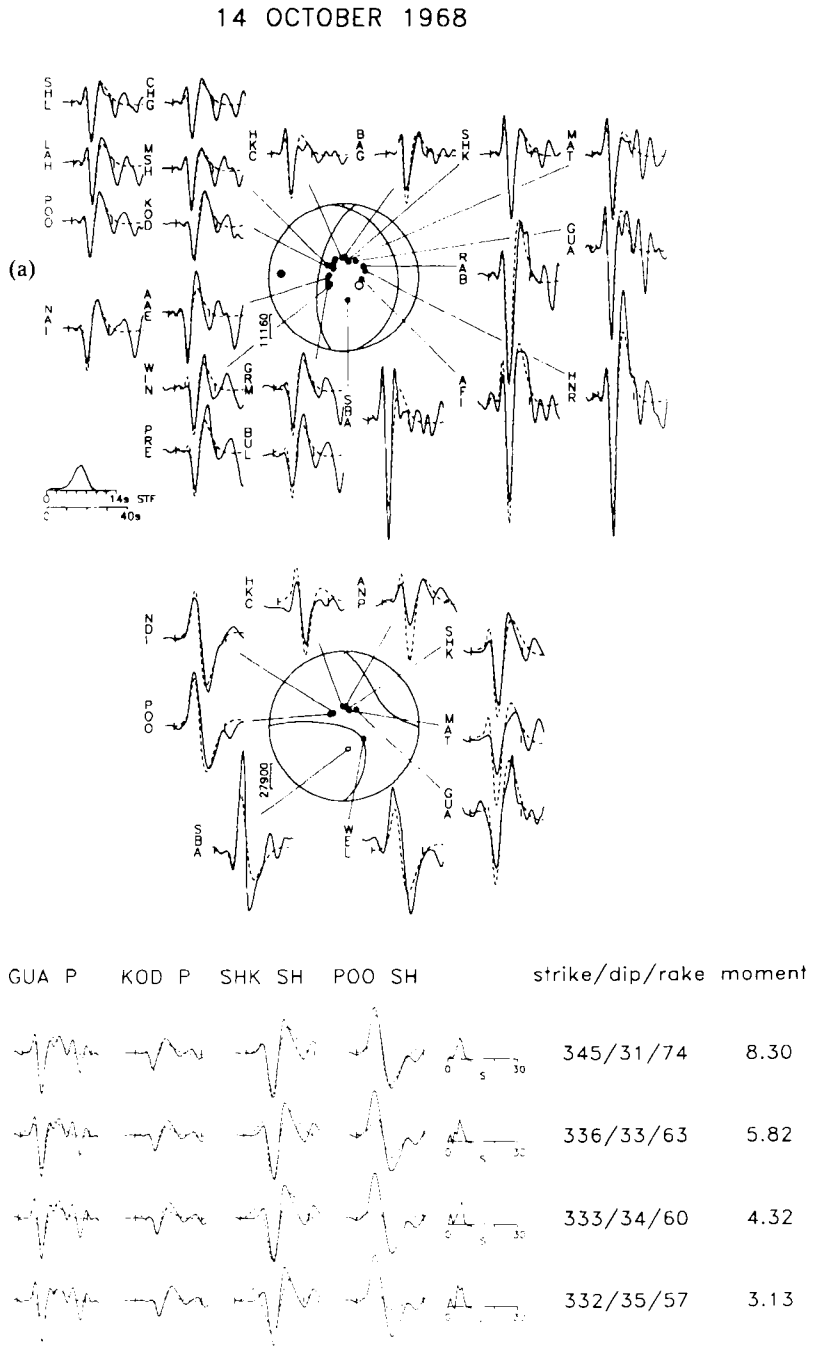

Figure 2. (a) Fault plane solution for the 1968 October 14 Meckering earthquake. Focal spheres and observed (solid) and synthetic (dashed) WWSSN long-period seismograms for the *P* (top) and *SH* (bottom) waves are shown. The amplitude axis (in microns) is for the seismograms adjusted to a common epicentral distance of 40° and WWSSN instrument magnification of 3000. The lower time scale is for the seismograms and the normalized source time function (STF) is shown on the upper time scale. The larger solid and open circles denote the *P*- and *T*-axes, respectively (b) Observed waveforms for the 1968 event compared to seismograms calculated at different centroid depths. For each test the centroid depth was fixed and the other parameters were determined by inversion. Depth is in kilometers and seismic moment in 10^{18} Nm. Note that the mechanism changes little with depth.

strike, dip, and rake of the fault plane are 7°, 1°, and 5°, respectively), and an identical centroid depth.

Uncertainties in the centroid depth are estimated by fixing the depth at a specified value, solving for the remaining parameters, and comparing the resulting seismograms to the data (Fig. 2b). For this mechanism, seismic moment decreases when the assumed depth is increased because the *P* and *pP* phases are of opposite polarity and therefore interfere less destructively as they become more separated in time. However, the up and down going *SH* phases are typically of the same polarity and therefore interfere constructively at shallow depths. Hence, for a deeper centroid, the amplitude of the *P*-waves can be matched by decreasing the seismic moment but this causes a misfit between synthetic and observed *SH* amplitudes. The *P*- and *SH*-waveforms constrain the centroid to be above 6 km and are matched best at 2.8 km.

The observed surface displacement and seismic moment constrained by the waveforms also suggest a very shallow centroid. The relation between seismic moment M_0 and average slip u is given by $M_0 = \mu ulw$ (Aki & Richards 1980), where μ is the shear modulus (the shear wave velocity squared × density; Table 2), and l and w are the length and width of a rectangular fault. Using M_0 as determined by the inversion (Table 1) and a downdip width equal to twice the centroid depth (Table 1) divided by the sine of the dip angle (Table 1), we obtain an average slip of 0.75 m. Assuming a semi-circular fault which intersects the surface with a cord length equal to l would increase the calculated slip value by 50 percent. In either case, the calculated average slip is much less than that observed at the surface trace of the fault. Except for the possibility that not all of the measured slip occurred during the earthquake or that the surface displacement was amplified by surface effects, the greater-than-average surface slip suggests that most of the slip was concentrated at shallow depths, implying a shallow centroid. For example, if we assume that the amount of slip decreases linearly from the observed average slip of 2 m at the surface to zero at 15 km depth, then the calculated seismic moment and dip angle indicate a centroid at about 2.4 km depth.

P-waveforms show a small precursor about 3.5 s prior to the main shock (Fig. 2a) which is clear on the short-period seismograms (Fitch *et al.* 1973; Vogfjord & Langston 1987). Fitch *et al.* (1973) noted that many of the first-motions recorded at regional distances for the first event were inconsistent with their solution for the main event and suggested that the precursor had a strike-slip mechanism. *P*-wave first-motions for the initial event on seismograms recorded at teleseismic distances are mostly indeterminate (see Vogfjord & Langston 1987). We modelled the earthquake initially as two separate events and found that long-period body waves were insensitive to the amount of strike-slip included for the first subevent. The precursory event is shown here as a small ramp in the source time function and the mechanism is presumed to be the same as that of the main event (Fig. 2a). This produces an acceptable fit to the beginning of most of the waveforms. The slight misfit of the *P*-waves to the SW (WIN, PRE, GRM and BUL) suggests that the dip angle may have changed slighly but this feature cannot be resolved with confidence. The inclusion of the precursor in our solution results in an approximately 25 per cent greater seismic moment (Table 1) than that found by Vogfjord & Langston (1987), who did not include the precursor.

3.2 Event 2: 1979 June 2, Cadoux

The 1979 Cadoux earthquake occurred less than 100 km from the epicenter of the 1968 Meckering event (Fig. 1) and was accompanied by surface faulting in a N-trending area roughly 15 km long and 3 km wide. The maximum observed displacement was 1.5 m (Lewis *et al.* 1981), so that the maximum and average slips (assuming a 30° dip) were probably about 3 m and 1.5 m, respectively. In contrast to the Meckering event, a west-side-up sense of relative slip was observed. The mechanism is similar to that for the Meckering earthquake except that it is rotated 20° counterclockwise and the shallow-dipping nodal plane dips to the west. This W-dipping nodal plane is most likely the fault plane. Uncertainties in the focal mechanism are comparable to those for the 1968 event. The effects of varying the centroid depth are similar to those discussed above for the Meckering earthquake, and we see again that the observed waveforms are best matched with a shallow centroid, most likely above 4 km. Using a calculation for a rectangular fault similar to that described above, we find that the estimated moment (Table 1) is consistent with an average slip of 0.3 m on a fault 15 km long and 6 km deep (i.e. twice the estimated centroid depth). As was found for the Meckering event, the average slip estimated from the seismic moment is much less than that observed at the surface.

3.3 Event 3: 1986 March 30, Marryat Creek

The 1986 Marryat Creek earthquake occurred in central Australia in a region showing little evidence of previous seismic activity (Fig. 1). The earthquake was accompanied by surface faulting on an L-shaped thrust fault. The arms of the L extended west and south from the apex and the southwest quadrant moved up relative to the surrounding area. The maximum throw of 0.6 m occurred at the apex while horizontal displacements of 0.1 m (left-lateral) and 0.25 m (right-lateral) occurred on the W-trending and S-trending arms, respectively (McCue *et al.* 1987).

Our solution is based on simultaneous inversion of long period *P*- and *SH*-waves and short-period *P*-waves (Fig. 4). We find an almost pure thrust mechanism at a centroid depth between 0 and 3 km. The observed surface faulting suggests that the SW-dipping *P*-wave nodal plane corresponds to the fault plane. Using a method similar to that described above for the 1968 earthquake, we find that the estimated seismic moment (Table 1) is consistent with an average slip of 0.3 m on a rectangular fault 13 km long and 3 km deep. In contrast to the Meckering and Cadoux earthquakes, this average slip is comparable to the slip measured at the surface. Uncertainties in the strike, dip, and rake angles are ±20°, ±20°, and ±25°, respectively.

3.4 Event 4: 1970 March 24, Canning Basin

The 1970 Canning Basin earthquake occurred in the western region of the continent (Fig. 1) in an area with no evidence

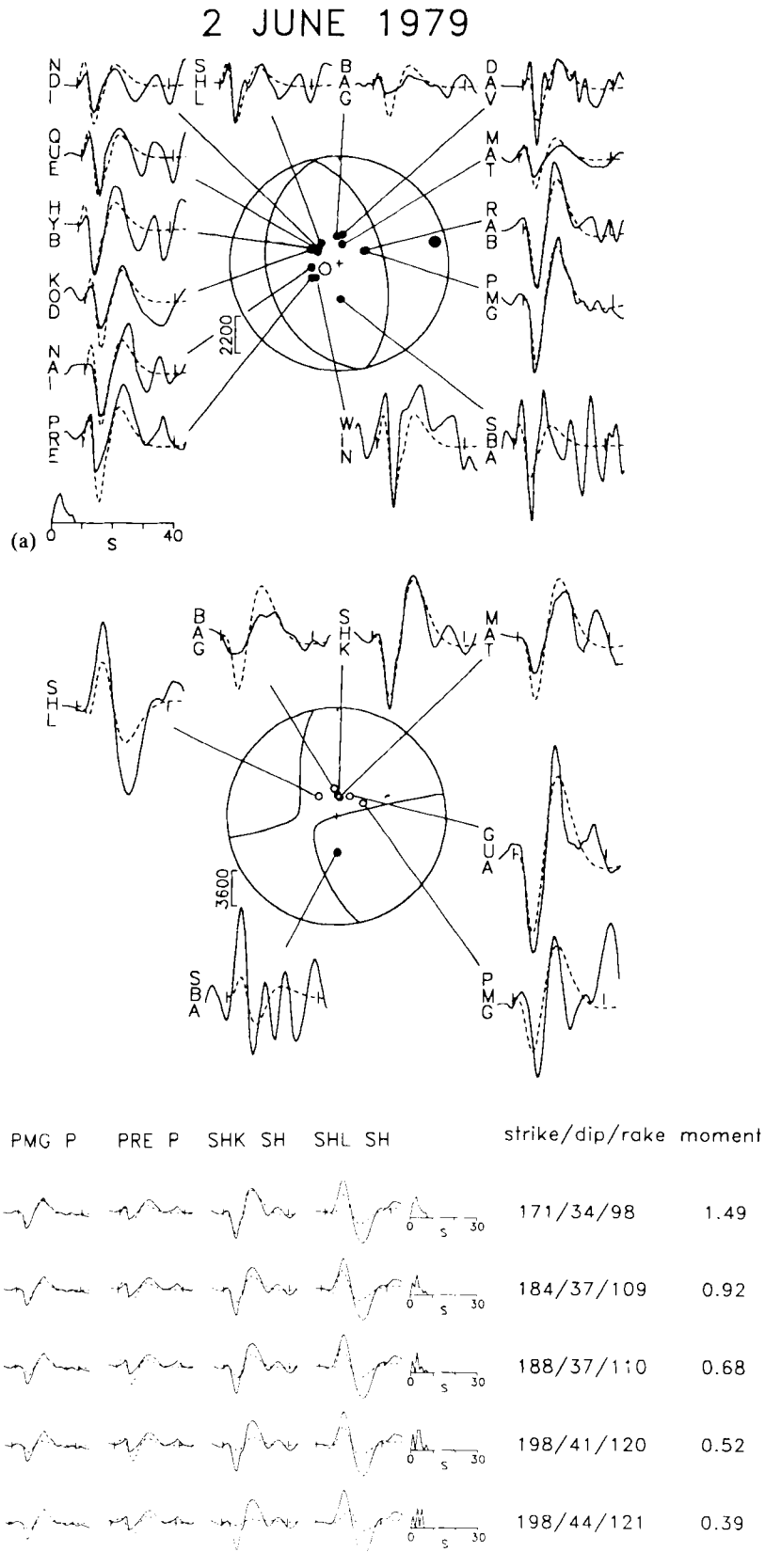

Figure 3. (a) Fault plane solution and WWSSN long-period seismograms for the 1979 June 2 Cadoux earthquake. The normalized source time function is shown on the time scale. See Fig. 2 for details. (b) Observed waveforms for the 1979 earthquake compared to synthetic seismograms calculated at different centroid depths. The results are similar to those found for the 1986 event (see text and Fig. 2 for details).

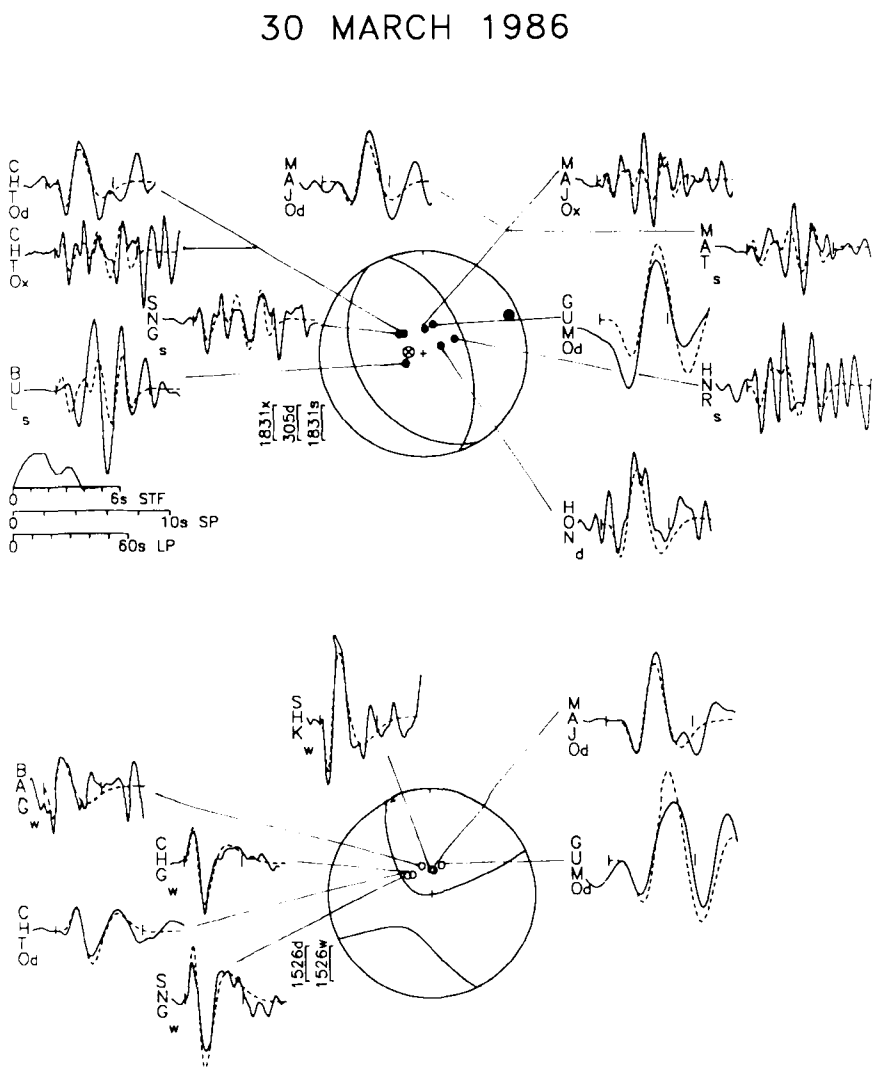

Figure 4. Fault plane solution and waveforms for the 1986 March 30 earthquake. The small 'w' and 's' indicate long- and short-period WWSSN data, respectively, while the 'd' and 'x' denote long- and short-period GDSN data, respectively. Amplitude scales, as described in Fig. 2, are shown for each data type. Separate time scales are shown for the long-period (LP) and short-period (SP) waveforms, and for the normalized source time function (STF). See Fig. 2 for details.

of previous seismicity or recent tectonic activity. The epicentral region is covered by Quaternary sediments and no fault scarp was observed. As many as 200 aftershocks occurred along a NW-trending zone in the two years following the main shock (Denham *et al.* 1974).

Our solution (Fig. 5) reveals almost pure thrust faulting on a plane striking roughly north. This event is different from the shallower events discussed above in its depth and also in that both of its nodal planes are steep. It is similar to the 1982 New Brunswick, Canada earthquake both in mechanism and depth, although its moment is roughly twice as large (e.g. Choy *et al.* 1983; Nabelek 1984). By constraining each parameter separately and solving for others, it was found that changes in the strike, dip, and rake angles of 5°, 10°, and 5°, respectively, considerably degraded the visual fit to the observed waveforms—these are our estimated uncertainties. Similarly, the centroid depth is constrained to 8 ± 3 km, indicating that the event occurred in the upper crust. Our solution is slightly different from the first motion solutions of Fitch *et al.* (1973) and Denham, Everingham & Gregson (1974) which included small components of strike-slip along planes striking NW or NNW.

3.5 Event 5: 1972 August 28, Simpson Desert

The 1972 Simpson Desert earthquake occurred in central Australia in a region that had previoulsy been the site of several large earthquakes (Fig. 1). No fault scarp was observed, but in the following four months 15 aftershocks occurred along a NE-trending zone (Stewart & Denham 1974).

This earthquake is the smallest of the events examined here (Table 1). The signal to noise ratios in *SH*-waveforms were too small for them to be modelled. *P*-waveforms constrain the mechanism to be a thrust, but they are insensitive to the strike of the nodal planes. We use *P*-wave first motions picked from short-period seismograms and the

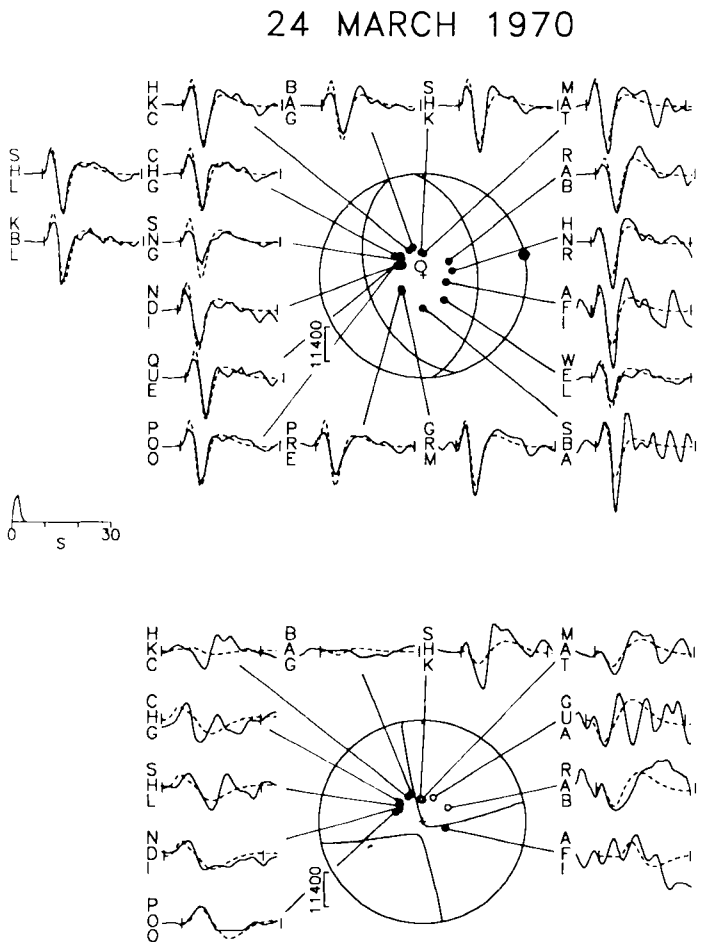

Figure 5. Fault plane solution and WWSSN seismograms for the 1970 March 24 Canning Basin earthquake. The normalized source time function is shown on the time scale. See Fig. 2 for details.

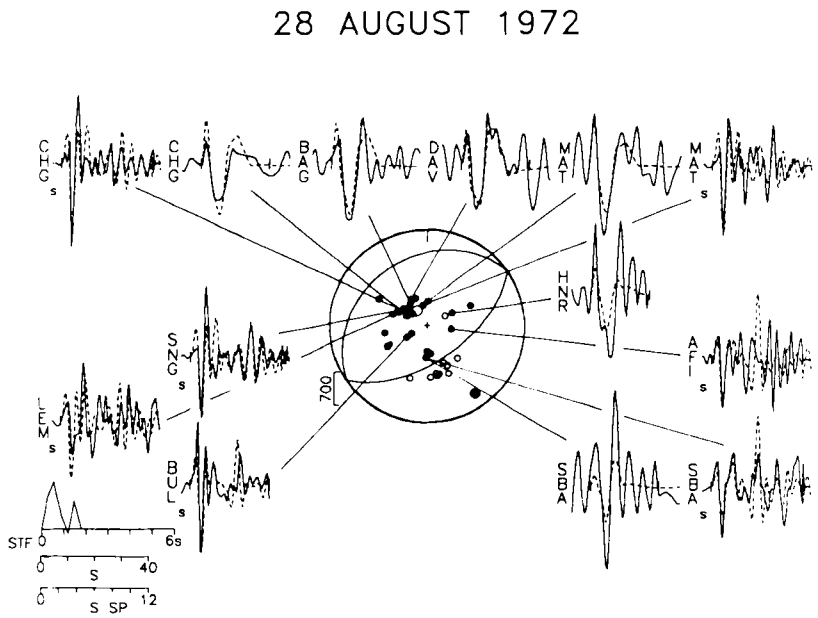

Figure 6. Fault plane solution and WWSSN *P*-wave seismograms for the 1972 August 28 Simpson Desert earthquake. Short-period compressional *P*-wave first motions are shown with closed circles and dilations are shown with open circles. An 's' indicates short-period data. The lower time scale is for the short period seismograms (SP), the middle for the long period seismograms, and the upper for the normalized source time function (STF). The observed and synthetic short-period seismograms are normalized by their corresponding rms amplitudes. See Fig. 2 for other details.

trend of the aftershocks to infer the strike and dip of the SE-dipping nodal plane (Fig. 6) and presumed a rake angle of 90°. With the mechanism fixed and the amplitudes of the seismograms normalized by their root-mean-squared amplitudes (McCaffrey & Nabelek, 1984), we inverted the long and short period *P*-waves simultaneously for the centroid depth and source time function. The seismic moment was determined from the amplitudes of the long-period *P*-waves.

Our solution is a thrust on a plane striking NE with a centroid depth of 8 ± 2 km. The strike, dip, and rake angles may vary by ±40°, ±10°, and ±40°, respectively, without violating the first motions or waveforms. Our solution differs from the first motion solution of Stewart & Denham (1974) who inferred a predominantly strike-slip mechanism with a nearly N-trending pressure axis. Short-period first motions picked by us, long- and short-period *P*-waveforms, and the small amplitudes of the *SH* relative to *P*-waveforms are all inconsistent with a strike-slip mechanism (strike-slip mechanisms produce *SH*-waveforms that are much larger than the *P*-waveforms, e.g. compare relative *P* and *SH* amplitudes for the two mechanisms in Figs 5 and 7).

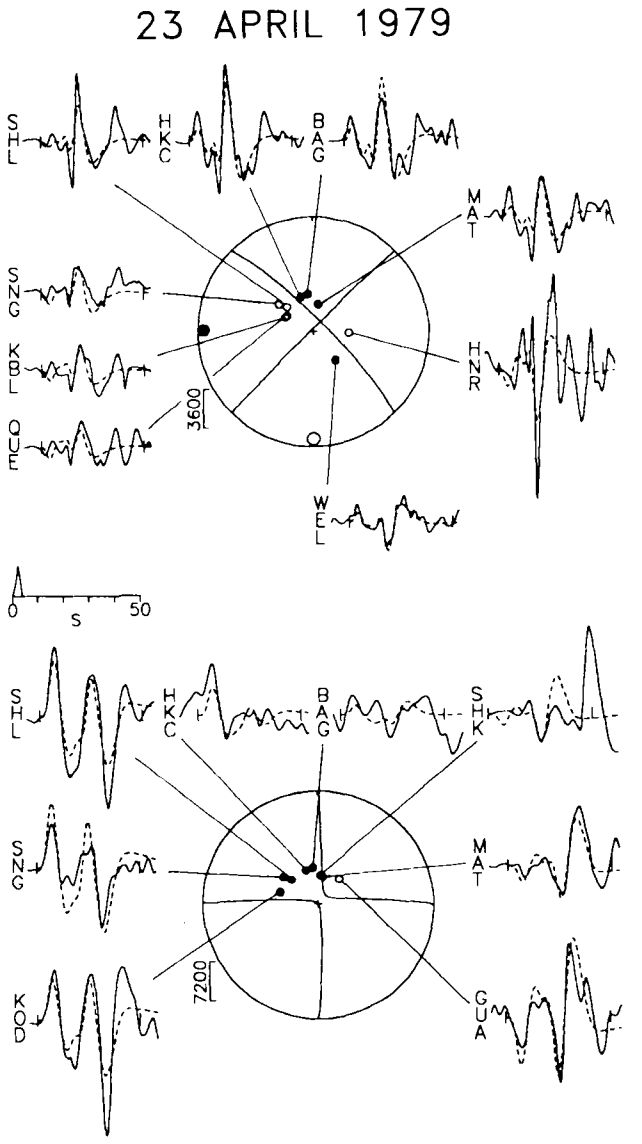

Figure 7. Fault plane solution and waveforms for the 1979 April 23 Broome earthquake. The normalized source time function is shown on the time scale. See Fig. 2 for details.

3.6 Event 6: 1979 April 23, Broome

The 1979 Broome earthquake occurred beneath a sedimentary basin about 300 km off the northwestern coast of Australia (Fig. 1). Previous activity in this region includes an event of magnitude greater than six in 1929. Over 50 aftershocks define a NW-trending zone roughly 100 km in length.

The crustal structure (Table 2) is taken from Stagg & Exon (1981) who inferred sediment thicknesses from seismic reflection profiles. Uncertainties in the strike, dip, and rake angles for our solution (Fig. 7) are less than 5°. The event was almost pure strike-slip and we favour the NW striking plane as the fault plane because it parallels the observed aftershock trend. The clear separation of the direct and reflected phases provides strong constraints on the centroid depth (27 ± 3 km). Estimates of crustal thickness in this area based on seismic reflection profiles are 25–30 km (Stagg & Exon 1981) and from this we infer that the earthquake occurred in the lower crust or uppermost mantle. The

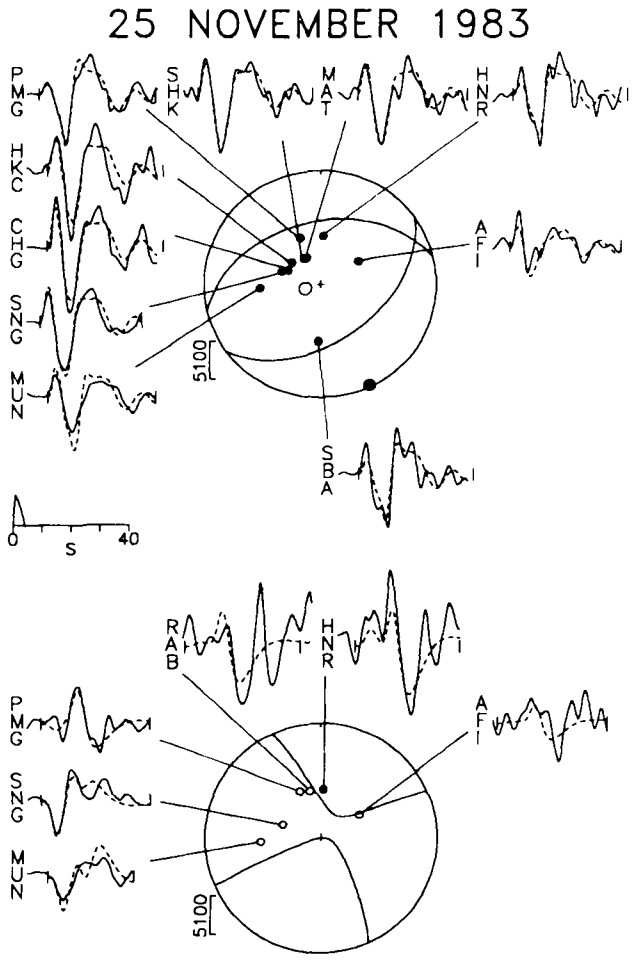

Figure 8. Fault plane solution and waveforms for the 1983 November 25 Tasman Sea earthquake. The normalized source time function is shown on the time scale. Note the latter part of both the observed and synthetic seismograms that include *P*-waves reverberating in the water layer. See Fig. 2 for details.

centroid-moment tensor solution of Dziewonski *et al.* (1987b) is similar to our solution.

3.7 Event 7: 1983 November 25, Tasman Sea

The 1983 Tasman Sea earthquake occurred beneath 4 km of water in oceanic lithosphere about 500 km off the southeast coast of Australia (Fig. 1). The central Tasman Sea was created by sea floor spreading in the interval 80–60 myr (Hayes & Ringis 1973). The region has been seismically active in the past, particularly in the period from 1883 to 1886 (Denham 1985).

Our solution (Fig. 8) shows almost pure thrust faulting on a NW- or SE-dipping plane. Uncertainties in mechanism are comparable to those for the 1970 event. The centroid depth (24 ± 2 km beneath sea level) indicates that the event took place in the upper mantle. Our solution is similar to that of Denham (1985) who used a *P*-waveform analysis technique and also to the centroid-moment tensor solution of Dziewonski, Franzen & Woodhouse (1984).

4 DISCUSSION

4.1 Strike-slip versus thrust faulting in the uppermost Australian crust

On the basis of published first motion solutions, Lambeck *et al.* (1984) suggest that a transition from strike-slip to thrust faulting occurs at about 5 km depth in southeastern Australia. For each of the three shallowest earthquakes presented above (events no. 1–3), published first motion solutions had large components of strike-slip motion and would possibly suggest a similar transition in western Australia. However, the waveform solutions found here indicate that thrust faulting occurs at even the shallowest depths in western Australia.

The strike-slip solutions are inconsistent with the waveform data (Fig. 9) which require predominantly thrust mechanisms with a shallow dipping fault plane. The centroid-moment tensor solutions for the Cadoux and Marryat Creek earthquakes (Dziewonski *et al.* 1987a, b) are similar to our solutions (Fig. 9). Moreover, in the first motion solutions for both the Cadoux event (Denham *et al.* 1985) and the main shock of the Meckering (Fitch *et al.* 1973) earthquake, the *P*-wave nodal plane whose azimuth is closest to the trend of the ground rupture predicts a sense of offset of the ground opposite to that observed. In our solutions these are the auxiliary planes. It is unlikely that the rupture initiated as strike-slip and became thrust because for all three events, it is the auxiliary plane that the strike-slip and thrust solutions have in common (Fig. 9), not the fault plane, and would thus require that the fault plane rather than the slip direction change after initiation of rupture. While very large events may rupture multiple fault planes of different orientations (recall that the long period body waves for the 1968 event are insensitive to the

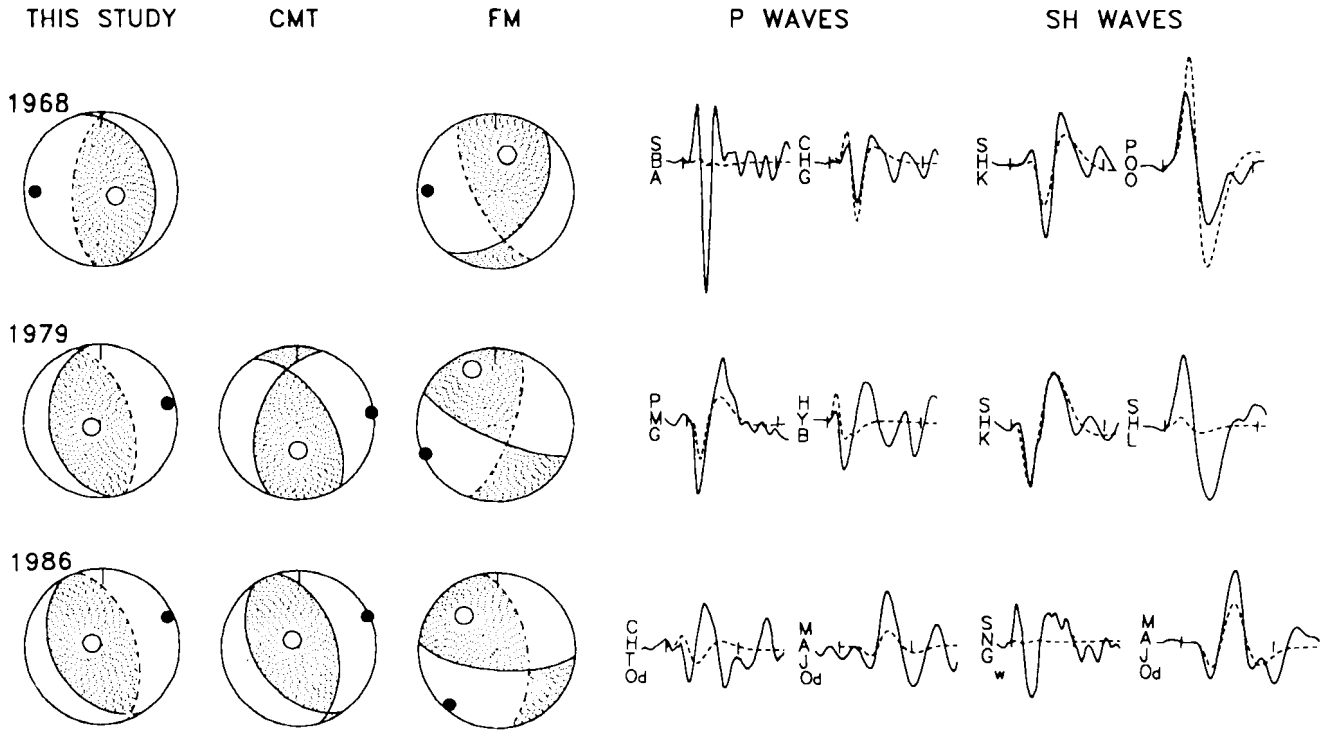

Figure 9. Comparison of published fault plane solutions for the three shallowest earthquakes studied here. The first column shows our solutions; the second the centroid-moment tensor (CMT) solutions (Dziewonski *et al.* 1987a, b); and the third column shows the solutions based on *P*-wave first motions (FM) (Fitch *et al.* 1973; Denham *et al.* 1985; McCue *et al.* 1987). The latter in all cases indicate a significant component of strike-slip motion in contrast to the almost pure thrust solutions found here (Figs 2–4). To test whether or not the strike-slip first motion solutions are consistent with the waveform data, inversions were performed in which the mechanism was fixed at the first motion solution and the depth and the source time function were allowed to vary. The resulting synthetic waveforms are shown and demonstrate a much poorer fit for the strike-slip solutions than for the thrust solutions (Figs 2–4). The inferred auxiliary planes are shown with dashed lines in the first and third columns.

mechanism of the precursor), we think it is unlikely that all three of these earthquakes performed this feat.

The orientations of the steeper auxiliary planes are constrained well (except as noted below) by first motions because the take-off angles of rays that leave the source steeply have small uncertainties. In the first motion solutions, the fault planes, that in our interpretation dip at angles of 30°–35°, are constrained largely by rays that travel through the uppermost mantle and crust and are recorded at regional distances. The take-off angles of these rays will have large uncertainties (i.e. tens of degrees) due to uncertainties in both their ray parameters and the seismic velocity at the source. Furthermore, lateral velocity variations will result in uncertainties in take-off azimuths. When there are large uncertainties in the positions of the rays on the focal sphere, first motions will become mixed and strike-slip solutions will result in the fewest first-motion violations.

The first motion solution of the Marryat Creek earthquake includes one nodal plane which is consistent with the ground rupture (McCue *et al.* 1987) but is inconsistent with the waveforms (Fig. 9). Our interpretation is that the average fault plane strikes NW–NNW, not parallel to either of the surface breaks, and that the slip vector is ENE directed. This solution gives the appropriate sense of displacement on both limbs of the surface break and is consistent with the waveform data. It does violate some first motions from regional *P*-waves (McCue *et al.* 1987) but for the reasons noted above we consider this to be of little consequence. Our solution is very similar to the best-fit double-couple solution of Dziewonski *et al.* (1987a) (Fig. 9).

The first motion solutions of the Meckering and Cadoux earthquakes have N-trending auxiliary planes that dip at angles of 8° and 15° greater than those that result from waveform analyses. We suggest that this is a systematic bias resulting from the interference between direct and reflected phases for very shallow events. For some stations, which project well into the compressional quadrant of the *P*-wave focal sphere (e.g. AAE and KOD in Fig. 2a), the amplitude of the *P*-wave first motion is very small, and perhaps even dilatational. For dip-slip events with a gently dipping fault plane, stations that fall in the compressional quadrant but near the auxiliary plane have a reflected phase *pP* opposite in polarity to and greater in amplitude than the direct phase *P*. For a very shallow source, the two phases arrive almost simultaneously and interfere destructively so that some stations in the compressional quadrant appear to have dilatational first motions. This apparent shrinkage of the quadrants was first observed by Langston (1976) for the 1967 Koyna, India earthquake and later by Hart (1978) and Trehu, Nabelek & Solomon (1981) for mid-ocean ridge earthquakes. While this effect can be lessened by using short-period seismograms in which the phases will be more clearly separated in time, it will be enhanced by background noise because *pP* is more conspicuous near the *P*-wave node.

4.2 Constraints on the regional intraplate stress field

The earthquakes studied here comprise the seven largest in and near the Australian continent in the past twenty years and provide important constraints on the regional intraplate stress field. For these large earthquakes, thrust faulting is clearly dominant (Fig. 1); of the seven earthquakes studied only one did not have a thrust mechanism. We discuss our solutions in terms of the pressure (*P*) axis because this axis is nearly horizontal for all of the events (Fig. 1).

The 1968 Meckering and 1979 Cadoux earthquakes in southwestern Australia are similar to each other in mechanism (except that their fault planes dip in opposite directions) and centroid depth (<5 km). They have E-trending *P*-axes. The 1970 Canning Basin earthquake in the western region occurred at a greater depth (although still in the upper crust) and had a similar *P*-axis. The 1979 Broome event northwest of Australia was a strike-slip event that occurred at a significantly greater depth, in the lower crust or uppermost mantle. The *P*-axis for this event is also horizontal and trends E; however, the tension and intermediate axes have traded directions with respect to the other western Australia events. The 1986 Marryat Creek event in central Australia was a shallow thrust and the orientation of the *P*-axis is very similar to that of the four earthquakes in the western region. The 1972 Simpson Desert was a thrust event and occurred in the upper crust in central Australia. However, due to the large uncertainties in the strikes of the nodal planes for this event, it is unclear whether or not the large difference in the *P*-axis trend between this and the other earthquakes is significant (Table 1, Fig. 1). The 1983 November event occurred in the upper mantle of oceanic lithosphere beneath the Tasman Sea and has a nearly horizontal *P*-axis oriented roughly NNW. To summarize, the pressure axis is consistently near-horizontal, and in the western region, five earthquakes indicate that the azimuth of the maximum compressive stress (σ_1) is E–ENE (azimuthal range of 66°–91°). The single event beneath the Tasman Sea indicates a NNW-trend.

The existence of a roughly E-trending horizontal maximum compressive stress (σ_1) in western Australia may be primarily a consequence of the resistance of the Indian Ocean–Australian plate to subduction along its northern margin (particularly at the Himalayan collision zone), as originally suggested by Fitch *et al.* (1973). The orientation of σ_1 (inferred from fault plane solutions) changes smoothly from roughly N in the Indian Peninsula to NW in the northeastern Indian Ocean to roughly E in western Australia (Fitch *et al.* 1973; Weissel *et al.* 1980; Bergman & Solomon 1980, 1985; this study). This variation is predicted by the global plate tectonic stress model E4 of Richardson, Solomon & Sleep (1979) in which the only plate boundary forces considered are at continental convergence zones. Model E31 of Richardson *et al.* represents an attempt to find a best model (rather than a limiting model) and is more realistic in that the plates are driven by symmetric forces at ridges and continental convergence zones and by drag forces on the base of the lithosphere. Model E31, however, predicts horizontal, NE-trending maximum compressional stresses for much of western, central, and eastern Australia. However, on the basis of the focal mechanisms found here, we conclude that the orientation of σ_1 is E throughout the western region, and possibly NW–NE in east-central Australia, and NNW beneath the Tasman Sea (Fig. 1).

Cloetingh & Wortel (1985) present an analysis similar to that of Richardson *et al.* (1979) but limit it to the stress field

in the Indian Ocean–Australian plate. Although they predict the systematic N–NW–E variation in the azimuthal orientation of σ_1 discussed above, their model does not predict our observations of the orientation of σ_1 in central Australia and beneath the Tasman Sea. Specifically, Cloetingh & Wortel predict the existence of horizontally oriented tensional stresses in much of eastern Australia. This result may be due to the large value assigned to the slab pull forces active at the Tonga–Kermadec trench.

The intraplate stress field off the northern coast of Australia may be influenced by forces associated with the subduction of the Indian Ocean–Australian plate along the Sunda Arc. The great Sumba earthquake of 1977 (Stewart 1978) suggests the presence of a large slab pull force here. A possible explanation for the transition from thrust to strike-slip faulting observed northwest of Australia is that the forces due to slab pull (oriented N, perpendicular to the local strike of the arc) reduce the magnitude of the intermediate compressive stress, σ_2, (oriented N), in effect causing a swap in the orientations of σ_2 and σ_3, and consequently, a transition from thrust to strike-slip faulting.

5 CONCLUSIONS

We determined source mechanisms, depths, seismic moments, and source time functions for the seven largest earthquakes in Australia in the past twenty years using teleseismic body waves. Five of the earthquakes show thrust faulting in the upper 10 km of the Australian crust. Three events had centroid depths of less than 5 km and produced surface rupture. Deeper earthquakes occurred offshore northwest Australia (strike-slip at 26 km depth) and offshore southeast Australia beneath the Tasman Sea (thrust at 24 km depth). It is likely that both of these were in the upper mantle.

First motion solutions for the Meckering (Fitch *et al.* 1973), Cadoux (Denham *et al.* 1985), and Marryat Creek (McCue *et al.* 1987) earthquakes include large components of strike-slip motion, whereas waveforms require thrust mechanisms and preclude large amounts of strike-slip motion. The gently dipping fault planes are not adequately resolved by *P*-wave first motions probably because they are constrained by regional phases whose take-off angles are poorly known. In addition, we find that the interference between the reflected and direct phases due to source shallowness results in apparent steepening of the auxiliary plane in first motion solutions.

The pressure axis is consistently near-horizontal, and in the western region five earthquakes indicate that the azimuth of the maximum compressive stress (σ_1) is E–ENE (azimuthal range of 66°–91°). Beneath the Tasman Sea, the *P*-axis is oriented NNW. The existence of E-trending compressional stresses in western Australia may result from the collision of the Indian continent with Asia. We suggest that the transition from thrust to strike-slip faulting along the northern margin of Australia is caused by increased slab pull forces at the Java trench.

ACKNOWLEDGMENTS

The manuscript was improved through comments and suggestions of G. Choy and J. Boatwright. JF thanks G. Abers for discussion and technical assistance. This project was initiated when RM visited B.M.R. in Australia with partial funding from the Department of Earth, Atmospheric, and Planetary Sciences, M.I.T. (thanks to Bill Brace), NSF Grant EAR84-20860, and the Bureau of Mineral Resources.

REFERENCES

Aki, K. & Richards, P. G., 1980. *Quantitative Seismology, Theory and Methods*, W. H. Freeman, San Francisco.

Bergman, E. A. & Solomon, S. C., 1985. Earthquake source mechanisms from body-waveform inversion and intraplate tectonics in the northern Indian Ocean, *Phys. Earth planet. Int.*, **40,** 1–23.

Bergman, E. A. & Solomon, S. C., 1980. Oceanic intraplate earthquakes: implications for local and regional intraplate stress, *J. geophys. Res.*, **85,** 5389–5410.

Bock, G. & Denham, D., 1983. Recent earthquake activity in the Snowy Mountain region and its relationship to major faults, *J. Geol. Soc. Aust.*, **30,** 423–429.

Choy, G. L., Boatwright, J., Dewey, J. W. & Sipkin, S. A., 1983. A teleseismic analysis of the New Brunswick earthquake of January 9, 1982, *J. geophys. Res.*, **88,** 2199–2212.

Cloetingh, S. & Wortel, R., 1985. Regional stress field of the Indian plate, *Geophys. Res. Lett.*, **12,** 77–80.

Denham, D., 1985. The Tasman Sea earthquake of 25 November 1983 and stress in the Australian plate, *Tectonophys.*, **111,** 329–338.

Denham, D., Alexander, L. G., Gregson, P. J., Wallance, T. C. & Enever, J., 1985. Intraplate stress and the 1979 Cadoux earthquake (abstract), *Bur. min. Rec. J. Aust. Geol. Geophys.*, **31,** 33.

Denham, D., Alexander, L. G. & Worotnicki, G., 1979. Stresses in Australian crust: evidence from earthquakes and *in situ* stress measurements, *Bur. min. Rec. J. Aust. Geol. Geophys.*, **4,** 289–295.

Denham, D., Everingham, I. B. & Gregson, P. J., 1974. East Canning basin earthquake, March 1970, *J. Geol. Soc. Aust.*, **21,** 353–358.

Doyle, H. A. & Underwood, R., 1965. Seismological stations in Australia, *Aust. J. Sci.*, **28,** 40–43.

Dziewonski, A. M. & Woodhouse, J. H., 1983. An experiment in systematic study of global seismicity: centroid-moment tensor solutions for 201 moderate and large earthquakes of 1981, *J. geophys. Res.*, **88,** 3247–3272.

Dziewonski, A. M., Franzen, J. E. & Woodhouse, J. H., 1984. Centroid–moment tensor solutions for October–December, 1983, *Phys. Earth planet. Int.*, **34,** 129–136.

Dziewonski, A. M., Ekstrom, G., Franzen, J. E. & Woodhouse, J. H., 1987a. Centroid-moment tensor solutions for January–March 1986, *Phys. Earth planet. Int.*, **45,** 1–10.

Dziewonski, A. M., Ekstrom, G., Franzen, J. E. & Woodhouse, J. H., 1987b. Global seismicity of 1979: centroid–moment tensor solutions for 524 earthquakes, *Phys. Earth planet. Int.*, **48,** 18–46.

Fitch, T. J., Worthington, M. H. & Everingham, I. B., 1973. Mechanisms of Australian earthquakes and contemporary stress in the Indian ocean plate, *Earth planet. Sci. Lett.*, **18,** 345–356.

Futterman, W. I., 1962. Dispersive body waves, *J. geophys. Res.*, **67,** 5279–5291.

Gordon, F. R. & Lewis, J. D., 1980. The Meckering and Calingiri earthquakes October 1968 and March 1970, *Bull. Geol. Surv. West Aust.*, **126.**

Hart, R., 1978. Body wave studies of the September, 1969, North Atlantic Ridge earthquake (abstract), *Eos, Trans. Am. Geophys. Un.*, **59,** 1135.

Hayes, D. E. & Ringis, J., 1973. Seafloor spreading in the Tasman Sea, *Nature*, **243,** 454–458.

Jackson, J., 1980. Errors in focal depth determination and the depth of seismicity in Iran and Turkey, *Geophys. J. R. astr. Soc.*, **61,** 285–301.

Lambeck, K., McQueen, H. W. S., Stephenson, R. A. & Denham,

D., 1984. The state of stress within the Australian continent, *Annal. Geophys.*, **2,** 723–742.

Langston, C. A., 1976. A body wave inversion of the Koyna, India, earthquake of December 10, 1967, and some implications for body wave focal mechanisms, *J. Geophys. Res.*, **81,** 2517–2529.

Langston, C. A. & Helberger, D. V., 1976. A procedure for modelling shallow dislocation sources, *Geophys. J. R. astr. Soc.*, **42,** 117–130.

Lewis, J. D., Daetwyler, N. A., Bunting, J. A. & Moncrieff, J. S., 1981. The Cadoux earthquake, 2 June 1979, *Geol. Survey West Aust.*, Report 11.

McCaffrey, R., 1988. Active tectonics of the eastern Sunda and Banda arcs, *J. geophys. Res.*, submitted.

McCaffrey, R. & Nabelek, J., 1984. The geometry of back arc thrusting along the eastern Sunda arc, Indonesia: constraints from earthquake and gravity data, *J. geophys. Res.*, **89,** 6171–6179.

McCue, K., Barlow, B. C., Denham, D. & Jones, T., 1987. Another chip off the old Australian block, *Eos, Trans. Am. Geophys. Un.*, **68,** 609.

Nabelek, J. L., 1984. Determination of earthquake source parameters from inversion of body waves, *PhD Thesis,* M.I.T., Cambridge, MA.

Nabelek, J., 1985. Geometry and mechanism of faulting of the 1980 El Asnam, Algeria earthquake from inversion of teleseismic body waves and comparison with field observations, *J. geophys. Res.*, **91,** 12713–12728.

Nelson, M. R., McCaffrey, R. & Molnar, P., 1987. Source parameters for 11 earthquakes in the Tien Shan, Central Asia, determined by P- and SH-waveform inversion, *J. geophys. Res.*, **92,** 12629–12648.

Richardson, R. M., Solomon, S. C. & Sleep, N. H., 1979. Tectonic stress in the plates, *Rev. geophys. Space Phys.*, **17,** 981–1019.

Stagg, H. M. J. & Exon, N. F., 1981. Geology of the Scott Plateau and Rowley Terrace, *Bur. min. Rec. Bull.*, **213,** 67 pp.

Stewart, G. S., 1978. Implications for plate-tectonics of the August 19 1977 Indonesian decoupling normal-fault earthquake (abstract), *Eos, Trans. Am. Geophys. Un.*, **59,** 326.

Stewart, I. C. F. & Denham, D., 1974. Simpson Desert earthquake central Australia, August 1972, *Geophys. J. R. astr. Soc.*, **39,** 335–341.

Stewart, I. C. F. & T. J. Mount, 1972. Earthquake Mechanisms in South Australia in relation to plate tectonics, *J. Geol. Soc. Aust.*, **19,** 41–52.

Sykes, L. R. & Sbar, M. L., 1973. Intraplate earthquakes, lithospheric stresses and the driving mechanism of plate tectonics, *Nature,* **245,** 298–302.

Trehu, A. M., Nabelek, J. L. & Solomon, S. C., 1981. Source characterization of two Reykjanes Ridge earthquakes: surface waves and moment tensors; P-waveforms and nonorthogonal nodal planes, *J. geophys. Res.*, **86,** 1701–1724.

Veevers, J. J. (ed.) 1984. *Phanerozoic Earth History of Australia,* Clarendon Press, Oxford.

Vogfjord, K. S. & Langston, C. A., 1987. The Meckering earthquake of 14 October 1968: a possible downward propagating rupture, *Bull. seism. Soc. Am.*, **77,** 1558–1578.

Weissel, J. K., Anderson, R. N. & Geller, C. A., 1980. Deformation of the Indo-Australian plate, *Nature,* **287,** 284–291.